NASA Technical Paper 3005

June 1990

Experimental Evaluation of a Tuned Electromagnetic Damper for Vibration Control of Cryogenic Turbopump Rotors

Eliseo DiRusso
and Gerald V. Brown

NASA

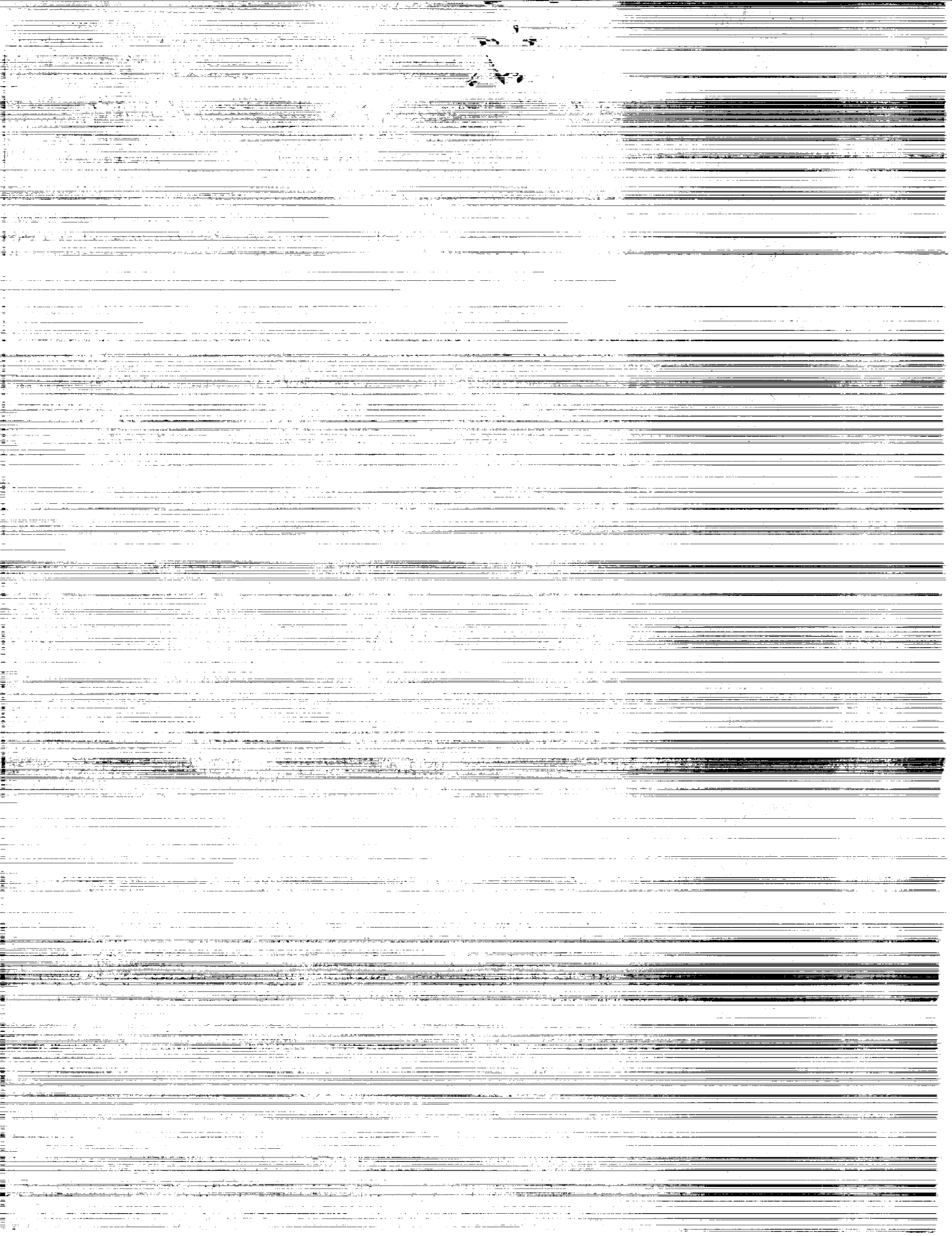

NASA Technical Paper 3005

1990

Experimental Evaluation of a Tuned Electromagnetic Damper for Vibration Control of Cryogenic Turbopump Rotors

Eliseo DiRusso
and Gerald V. Brown
Lewis Research Center
Cleveland, Ohio

National Aeronautics and Space Administration
Office of Management
Scientific and Technical Information Division

Summary

Experiments were performed on a tuned electromagnetic damper for damping rotor vibrations for possible applications in cryogenic turbopumps for rocket engines. The effectiveness of this damper improves as the temperature is reduced and is most effective in cryogenic applications where the temperatures are very low. Hence, it is not a viable damper at room temperature.

A test rig capable of speeds up to 14 000 rpm was used to simulate a turbopump rotor. Turbopump temperatures were produced in the rig with liquid nitrogen at −196 °C (−321 °F). The rotor was unbalanced and operated through its critical speed. The unbalance amplitude response of the rotor shaft was measured for undamped (baseline) and damped conditions at the critical speeds of the rotor (approximately 5900 to 6400 rpm).

The tuned electromagnetic damper utilizes an inductive, resistive, capacitive electrical circuit for maximizing the damping capability. This circuit requires tuning so that maximum damping is achieved at the mechanical vibration frequency to be damped.

It was found that the tuned electromagnetic damper can be effective in damping single mode, narrow bandwidth amplitude response. For multimode, closely spaced modes, or wide bandwidth amplitude response, the damper was less effective because it did not damp the response at the extremes of the response bandwidth where the amplitude was still high.

Introduction

Cryogenic turbomachinery used for pumping high pressure liquid hydrogen at −251 °C (−420 °F) or liquid oxygen at −179 °C (−290 °F) to the space shuttle main engines has experienced serious rotor instabilities. Reference 1 gives a description of the hydrogen turbopump for the space shuttle main engine and its associated rotor instabilities. Also discussed are the effects of seal stiffness and damping on rotor stability.

Conventional vibration dampers that utilize viscous fluids (such as bearing lubricating oil) cannot be used in turbopumps because oil congeals at cryogenic temperatures. Turbopump bearing compartments are filled with either liquid oxygen or liquid hydrogen, both of which have low viscosities and are therefore not effective fluids for viscous dampers (ref. 1). In addition, viscoelastic damping is limited because most viscoelastic materials tend to become hard and brittle in the cold turbopump environment. New methods for providing damping for cryogenic turbomachinery rotors are therefore necessary in dealing with rotor vibration and instability problems in the new generation of space shuttle main engines.

Electromagnetic damping shows promise in providing damping for turbopump rotors. This damper is a simple ac generator that removes energy from a vibrating system by converting the vibration energy into electrical current. The current flows through a resistive conducting material, causing the material to heat up. The heat generated in the material is dissipated to the surrounding environment which, in the case of cryogenic turbopumps, is either liquid hydrogen or liquid oxygen.

In order to be effective, this electromagnetic damper requires low temperatures such as those found in cryogenic turbopumps. It is not a viable damper at room temperature. This is because the lower resistance of copper at cryogenic temperatures (approximately one-seventh of room-temperature resistance at liquid nitrogen temperature) permits greater current to flow in the circuit, thereby greatly increasing the damping. Because low temperature is inherent in the turbopumps, it appears that electromagnetic damping is particularly well suited for damping rotor vibrations in cryogenic turbopumps.

The tuned electromagnetic damper is an extension of earlier research on eddy current dampers. In eddy current dampers, eddy currents are generated in an electrically conductive plate that vibrates in the presence of a magnetic field (ref. 2). This type of damper will produce a force opposite the plate motion for unidirectional motion (as in an eddy current brake) or at a low vibrational frequency (ref. 3). However, when the period of motion becomes shorter than the time constant L/R (inductance/resistance) for inductive decay, little resistive dissipation of induced currents can occur before the inducing emf changes sign; hence, the energy stored in the eddy current magnetic field is returned to the permanent magnet's magnetic field. At higher frequencies, the eddy current damper acts as a spring and dissipates very little energy. The frequency around which the transition from damping to springlike behavior occurs is lower for lower resistance. At cryogenic temperatures, that frequency can fall below values typically occurring in turbomachinery.

In the tuned electromagnetic damper, a voltage is induced in copper wire coils. This permits placement of the coils in

an electrical circuit to form an inductive, resistive, capacitive (LRC) circuit. This LRC circuit can be tuned to cancel out the springlike behavior so that it will produce maximum damping at the frequency of the mechanical vibration to be damped. The tuning process simply brings the alternating current into phase with the alternating voltage at a desired frequency (ref. 4), maximizing the current generated and consequently the power dissipated.

Experimental tests were performed on the tuned electromagnetic damper in a rig that simulated typical rotors and the cold environment of cryogenic turbopumps. The purposes of the tests were to—

(1) Experimentally evaluate the effectiveness of the tuned electromagnetic damper in damping rotor vibrations produced by rotor unbalance;

(2) Assess the feasibility of using electromagnetic dampers to damp rotor vibrations in cryogenic turbopumps; and

(3) Gain insight into the behavior of electromagnetic dampers for cryogenic turbopumps.

Symbols

A conductor cross-sectional area, m^2

C capacitance, F

c damping coefficient, n sec/m (lb sec/in.)

c_r damping coefficient at circuit resonant frequency, n sec/m (lb sec/in.)

E electromotive force, V rms

F force that opposes a displacement, n rms

f frequency, Hz

f_r resonant frequency of circuit, Hz

I current, A rms

L inductance, H

l length of conductor in magnetic field (projected perpendicular to motion), m (in.)

N number of conductors in magnetic field

P_d power dissipated in damping, W rms

P_e power dissipated in circuit, W rms

P_r power dissipated at circuit resonant frequency, W rms

R resistance, Ω

V volume of conductors in magnetic field, m^3

v vibratory velocity and velocity of conductor in plane normal to flux lines, m/sec rms

Z impedence, Ω

α ratio of length of conductor in magnetic field (projected perpendicular to motion) to total length of conductor in coil

β flux density, Wb/m^2

ρ resistivity of conductor, Ω m

Apparatus

Electromagnetic Damper Test Rig

The electromagnetic damper test rig simulates the rotors and the cold environment found in cryogenic turbopumps. It is used to evaluate the performance of electromagnetic vibration dampers in cryogenic turbopump applications. A schematic of the basic features of the rig is shown in figure 1, and a photograph of the electromagnetic damper installed in the test rig is shown in figure 2. The rig consists of a vertically oriented rotor supported on ball bearings. The lower bearing is supported by a flexible squirrel-cage spring. The rotor has a disk for simulating typical cryogenic turbopump rotors. It is driven by an ac motor through a belt and pulley speed increaser (2-to-1 ratio) and is capable of speeds up to approximately 14 000 rpm. The critical speed of the rotor was in the range from 5900 to 6400 rpm. The mode shape is a combination of first bending and displacement of the lower bearing housing.

The electromagnetic damper (fig. 2) is situated at the lower bearing housing. Its purpose is to damp lateral vibrations of the lower bearing housing. The damper and the bearing are both submerged in liquid nitrogen during tests. The purposes of the liquid nitrogen are to provide temperatures comparable to those found in cryogenic turbopumps and also to provide the low temperature required for efficient damper performance. The liquid nitrogen level is automatically controlled by a liquid level-sensing system. A vacuum chamber (fig. 1) surrounds the liquid nitrogen vessel in order to reduce the liquid nitrogen boil-off rate by reducing heat transfer through the vessel walls.

The rotor has provision for unbalancing the disk by placing set screws near the outer periphery of the disk. Unbalancing the rotor causes high lateral displacement of the lower bearing housing at the critical speed. The purpose of this is to evaluate the performance of the electromagnetic dampers.

Tuned Electromagnetic Damper

The basic components of the tuned electromagnetic damper are shown in figures 3 and 4. These are the copper coils (fig. 3(a)), neodymium iron boron magnets (fig. 3(b)), and magnetic iron pole pieces. The tuning capacitor is not shown in the figure. The coils are cemented to a carrier plate that is rigidly attached to the bearing housing (fig. 4). These coils (each of which has four magnets) are situated within the magnetic field produced by the magnets located above and below the coils. The general arrangement and shape of the magnets and coils evolved from available hardware and are by no means optimum.

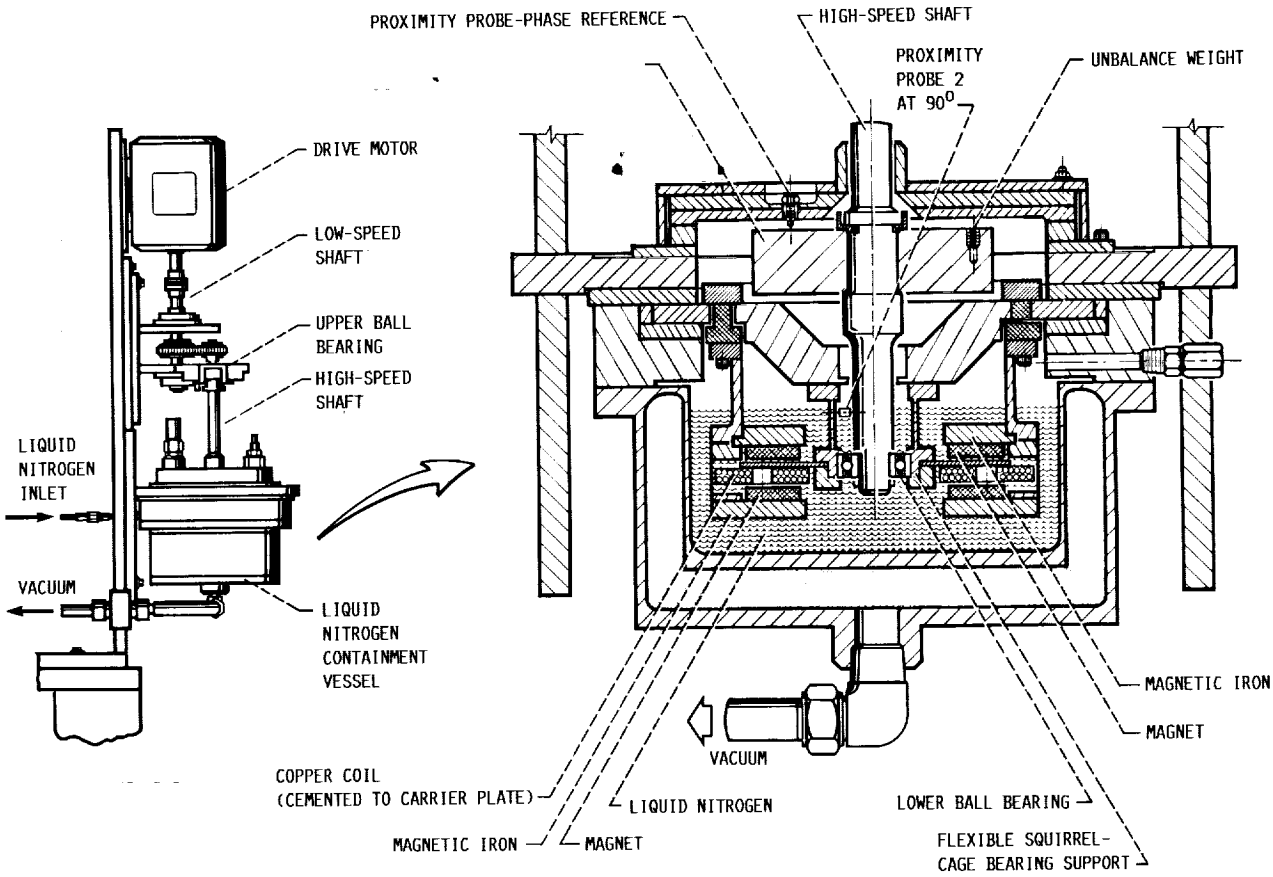

Figure 1.—Electromagnetic damper test rig (liquid nitrogen).

ORIGINAL PAGE
BLACK AND WHITE PHOTOGRAPH

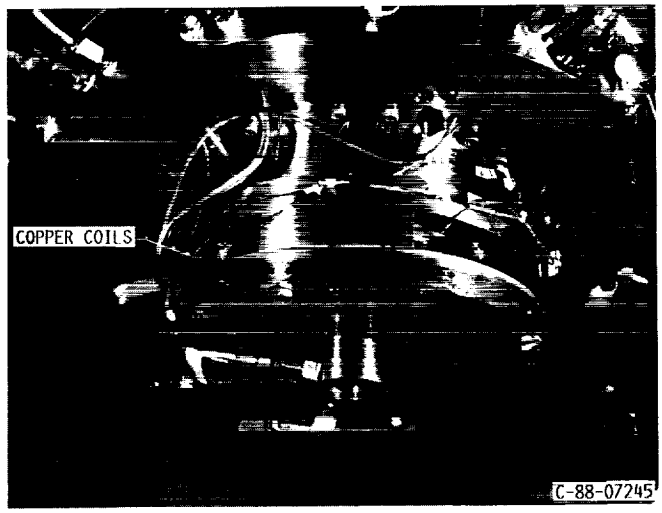

Figure 2.—Electromagnetic damper installed in test rig.

ORIGINAL PAGE IS
OF POOR QUALITY

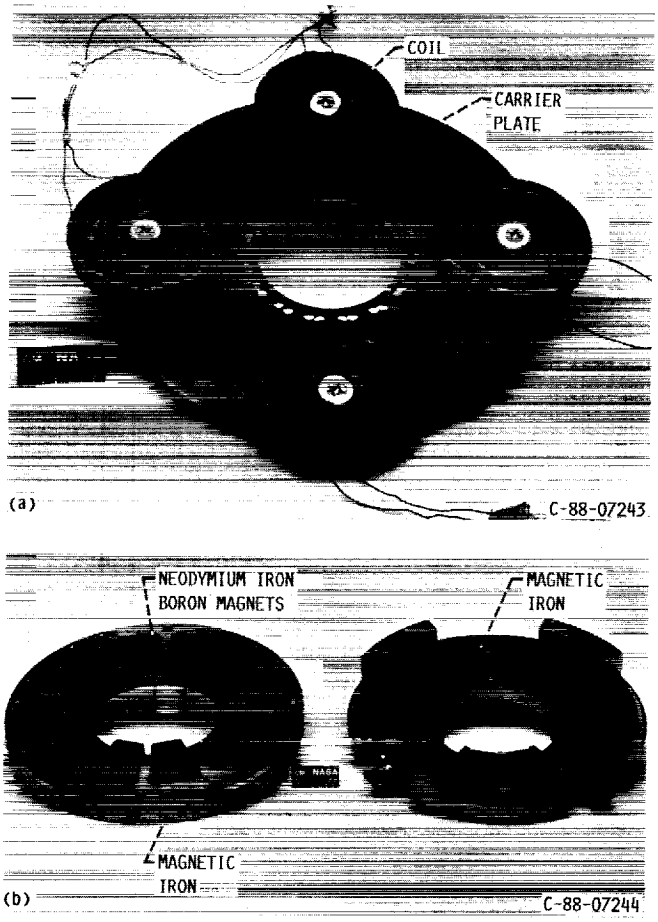

(a) Coil and carrier assembly.
(b) Magnet assembly.

Figure 3.—Photograph of electromagnetic damper components.

Each coil was wound in the form of an annulus. The coil size and number of turns were selected so that a maximum number of turns were within the magnetic fields of the magnets. The two coils which provided damping for the X' direction (see fig. 4) were connected in series, as were the two coils that provided damping for the Y' direction. This arrangement formed two independent dampers. It should be noted that the two coils on the X'-X' axis provide damping in the Y' direction, and the two coils on the Y'-Y' axis provide damping in the X' direction. The 15° angle (fig. 4) between the coil axis and the displacement measurement axis is caused by the physical constraints of the existing hardware. It does not affect damper operation but it does complicate data analysis. Table I outlines the physical and electrical specifications of the damper.

The electrical circuit for the tuned electromagnetic damper is shown in figure 5. Note that independent circuits are required for the X'-X' and Y'-Y' axes. The circuits were wired to facilitate remote on-line switching of the electromagnetic damper between the open circuit (undamped) and the tuned circuit with capacitors (damped) during any test.

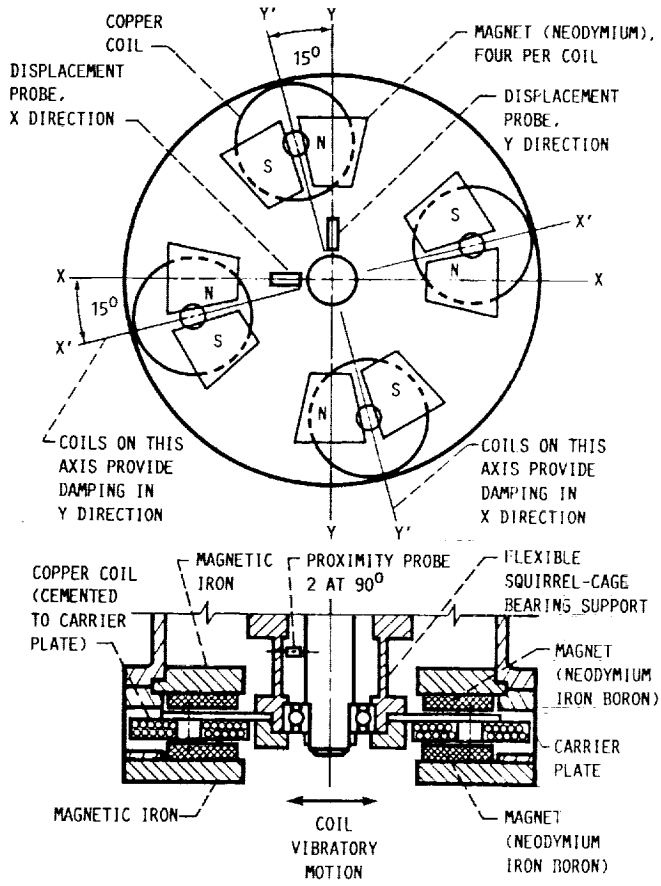

Figure 4.—Sketch of electromagnetic damper showing arrangement of copper coils, magnets, and displacement probes.

TABLE I.—PHYSICAL AND ELECTRICAL SPECIFICATIONS OF TUNED ELECTROMAGNETIC DAMPER

Coil wire material	Copper
Coil wire diam	24 gauge (0.56 mm, 0.022 in.)
Coil dimensions	
Outside diam	63.5 mm (2.5 in.)
Inside diam	12.7 mm (0.5 in.)
Thickness	9.7 mm (0.38 in.)
Total number of wire turns per coil	800 (approx.)
Effective number of wire turns in magnetic field of each magnet pair	500 (approx.)
Effective length of wire in magnetic field of each magnet pair (projected perpendicular to motion)	20 mm (0.8 in.)(approx.)
Coil resistance (2 coils in series)	13.2 Ω at 20 °C (68 °F) 1.9 Ω at −196 °C (−321 °F)
Coil inductance (2 coils in series)	0.026 H
Magnet material	Neodymium iron boron
Average magnetic field strength (measured in air gap)	6.2 kG at magnet corners 5.5 kG at magnet center 5.7 kG average
Air gap between magnets	17 mm (0.67 in.)
Capacitance (selected for desired tuned frequency)	90 or 100 μF

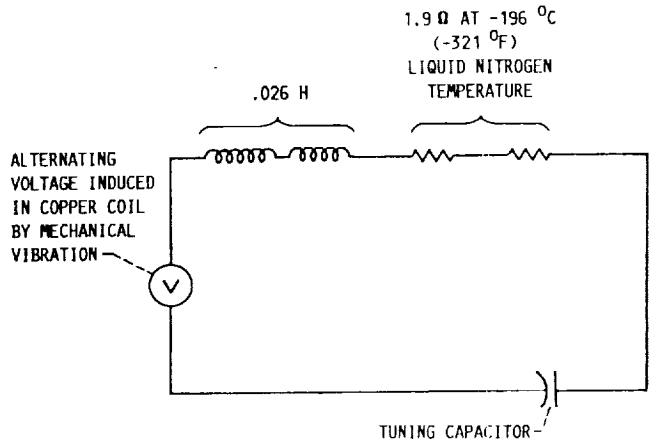

Figure 5.—Schematic diagram of electromagnetic damper circuit. (Each damping axis has this type of independent circuit.)

This enabled on-line comparison of damped with undamped conditions during tests.

Vibratory motion of the coils (fig. 4) within the magnetic field induces an alternating emf in the coils, causing an alternating current to flow in the circuit. The emf is induced under the footprint of each magnet pair. The net voltage generated in the circuit is therefore the sum of the four voltages induced in the coils between the four magnet pairs. The arrangement of the magnetic poles is also shown in figure 4.

Instrumentation

Instrumentation consisted of proximity probes (figs. 1 and 4) that measured lateral displacement of the shaft in two orthogonal directions. A third proximity probe located near the other two probes detected the change of probe output sensitivity between room temperature and liquid nitrogen temperature. This probe faced a notch of known depth (0.254 mm, 0.010 in.) in the shaft. The sensitivity at liquid nitrogen temperature was obtained by noting the change in probe voltage output as the notch passed by the probe. This voltage was divided by the known 0.254 mm (0.010 in.) notch depth to obtain the probe sensitivity at liquid nitrogen temperature. It was found that the probe sensitivity was reduced by a factor of approximately 2.7 in going from room temperature to liquid nitrogen temperature (−196 °C, −321 °F).

The probes were calibrated at room temperature. This factor was used to determine the calibration at liquid nitrogen temperature. A proximity probe facing the rotor disk (fig. 1) provided a once-per-revolution timing signal. The displacement and proximity probes had a nominal 0.76 mm (0.030 in.) gap to the shaft. Accelerometers mounted on an extension of the squirrel-cage housing were monitored during the tests but were not used for data analysis.

The current flow in the copper coils of the electromagnetic damper was obtained by measuring the voltage drop across a 50 mΩ series resistor in the circuit and then dividing the voltage drop by the resistance. A thermocouple mounted near the electromagnetic damper coils was used to monitor the temperature of the coils. The data signals from the instrumentation were stored on magnetic tape for subsequent processing by a computer data system.

Data System

The instrumentation signals from the magnetic tape were processed with an automated diagnostics computer program for rotating equipment. In this system, the two orthogonal shaft displacement signals and the once-per-revolution timing signal were passed through a digital vector filter that digitized and filtered the data to obtain only the response at the rotating speed (synchronous response). The system then computed the synchronous response and plotted it as a function of shaft speed in rpm.

Shaft orbits were obtained by feeding the two orthogonal shaft displacement signals from the magnetic tape to a waveform analyzer. This device sampled the time signals from the two orthogonal displacement probes at a given speed, digitized the data, and then stored it on floppy disks. A personal computer was then used to plot the Y displacement against the X displacement at a given speed to obtain shaft orbits at that speed.

Procedure

Prior to being tested, the rotor disk was unbalanced by placing set screws in tapped holes near the periphery of the disk. The unbalance used for all of the tests was 6.5 g-cm (0.09 oz-in.). This unbalance was selected because it produced reasonable amplitudes for evaluating the damper performance without causing excess vibration amplitude. The liquid nitrogen flow was then turned on (after the air was purged from the vessel by flowing gaseous nitrogen through it) and allowed to flow into the rig. The temperature at the copper coils was monitored as the liquid nitrogen flowed. After reaching −196 °C (−321 °F) liquid nitrogen temperature, the system was allowed to stabilize for approximately 5 min before commencing rotor rotation. This entire cooling process took approximately 20 min including the stabilization time. The rotor was then started and slowly accelerated through a speed range of 900 to 10 000 rpm. Data were recorded on magnetic tape for the entire speed range. In the region of the critical speeds, the rotor was accelerated slowly and was held at the critical speeds to ensure steady-state response data. Tests were performed for three cases. These were—

(1) No damping (baseline);

(2) Electromagnetic damper on and tuned for 103.4 Hz with 90 μF capacitor; and

(3) Electromagnetic damper on and tuned for 98.2 Hz with 100 μF capacitor.

Tuning of the electromagnetic damper circuit is discussed in the following sections.

Results and Discussion

Power Dissipated in Damper

The emf induced in the coils (fig. 5) causes a current to flow in the circuit. This current causes the coils to heat. (See the "Apparatus" section for a description of the electromagnetic damper). The heat is dissipated to the surroundings and produces damping of the vibratory motion.

The electrical power dissipated in the process is $P_e = I^2R$. In an ac circuit such as this, however, $I = E/Z$. Hence

$$P_e = \frac{E^2R}{Z^2} \tag{1}$$

The impedance (ref. 5) is

$$Z = \left[R^2 + \left(2\pi fL - \frac{1}{2\pi fC}\right)^2\right]^{1/2}$$

and the power dissipated becomes

$$P_e = \frac{E^2R}{\left[R^2 + \left(2\pi fL - \frac{1}{2\pi fC}\right)^2\right]} \tag{2}$$

Equation (2) shows that maximum power is dissipated when the term $[2\pi fL - 1/(2\pi fC)]$ is zero. Therefore, maximum power dissipation occurs when $2\pi fL = 1/(2\pi fC)$. The solution to this equation for f yields the resonant frequency of the electrical circuit as follows:

$$f = f_r = \frac{1}{2\pi(LC)^{1/2}} \tag{3}$$

At the resonant frequency of the circuit (f_r), the power dissipated becomes $P_r = E^2/R$. This shows that, at the resonant frequency, maximum power dissipation occurs and is inversely proportional to the coil resistance. In order to achieve maximum power dissipation at the frequency of a particular mechanical vibration, the circuit must be tuned to that frequency. Tuning is achieved by selecting the capacitance C according to equation (3) (see the appendix for the effects of varying the inductance, resistance, and capacitance).

Because the resistance of copper is greatly reduced at cryogenic temperatures, the damper is very effective at resonance at these temperatures. Note that the resistance of the coils at liquid nitrogen temperature was approximately one-seventh of the room-temperature resistance.

Theoretical Damping Coefficient

A theoretical damping coefficient may be derived from the electrical power dissipated in the circuit. The damping coefficient is defined as

$$c = \frac{F}{V} \tag{4}$$

Hence, $F = cv$. By multiplying this equation through by v, we obtain the power consumed in damping

$$P_d = Fv = cv^2$$

The equating of P_d to the power dissipated in the electrical circuit P_e (see eq. (2)) yields

$$cv^2 = \frac{E^2R}{R^2 + \left(2\pi fL - \frac{1}{2\pi fC}\right)^2}$$

and

$$c = \frac{E^2R}{v^2\left[R^2 + \left(2\pi fL - \frac{1}{2\pi fC}\right)^2\right]} \tag{5}$$

At electrical resonance, the damping coefficient becomes

$$c_r = \frac{E^2}{v^2R} = \frac{I^2R}{v^2} \tag{6}$$

The damping coefficient may also be expressed in terms of magnetic flux density, number of conductors in the coils, and length of conductors in the magnetic field. From reference 6, the voltage generated in the coils is

$$E = N\beta vl \tag{7}$$

Hence,

$$\frac{E^2}{v^2} = N^2\beta^2l^2$$

The substitution of this equation into equation (5) yields

$$c = \frac{N^2\beta^2 l^2 R}{R^2 + \left(2\pi fL - \frac{1}{2\pi fC}\right)^2} \tag{8}$$

Because the damping coefficient depends upon frequency, this type of damper is not a simple linear element. At the resonant frequency of the electrical circuit, this equation reduces to

$$c_r = \frac{N^2\beta^2 l^2}{R} \tag{9}$$

It should be noted that the flux density β is a function of the type and size of the magnets, the air gap between the magnets, and the physical arrangement of the magnets. Complex optimization studies involving these variables must be performed in order to maximize the flux density and thereby optimize damping performance.

It can also be shown that the damping coefficient is proportional to the volume of the conductors in the magnetic field V. From equation (9), at electrical resonance

$$c_r = \frac{N^2\beta^2 l^2}{R}$$

but

$$R = \frac{\rho l N}{A\alpha} \tag{10}$$

By substituting equation (10) into (9) we obtain

$$c_r = \frac{\beta^2 NAl\alpha}{\rho} = \frac{\beta^2 V\alpha}{\rho}$$

This shows that for maximum damping it is important to choose the coil/magnet geometry so that the volume of conductors in the magnetic field is maximized within the available space envelope and that the parameter α is maximized as well.

Effect of Temperature on Damping Coefficient

It is of interest to predict the behavior of the damping coefficient as a function of frequency for various temperatures. In equation (8), for a given damper configuration the quantities $N^2\beta^2 l^2$ and L and C do not change with temperature or frequency but R/Z^2 does. Note that the denominator in equation (8) is Z^2. Hence, the behavior of the damping coefficient can be obtained by plotting R/Z^2 as a function of frequency. Figure 6 is such a plot for room temperature, liquid nitrogen temperature, and liquid hydrogen temperature. The figure shows that at room temperature R/Z^2 has a low value and is relatively constant over the frequency range from 80 to 130 Hz. Note that at the tuned frequency (103.4 Hz), the value of R/Z^2, and hence the damping coefficient, increase significantly at liquid nitrogen temperature, and at liquid hydrogen temperature they are very high indeed. For frequencies above or below the tuned frequency, however, the value of R/Z^2 diminishes and eventually becomes less than the room-temperature value. Note also that the bandwidth over which R/Z^2 exceeds the room-temperature value is much less for liquid hydrogen temperature (approximately 4-Hz bandwidth) than for liquid nitrogen temperature (approximately 30-Hz bandwidth). This shows that whereas, at cryogenic temperatures, damping increases significantly near the tuned frequency, the bandwidth over which the damper is effective becomes narrower. The value for the resistance of copper at liquid hydrogen temperature for this analysis was 0.029 Ω (resistivity = 3.7×10^{-11} Ω m). This value of resistance was calculated by multiplying the room-temperature coil resistance of 13.2 Ω by the ratio of copper resistivity at liquid hydrogen temperature to resistivity at room temperature. Note that at liquid hydrogen temperature the coil resistance may not dominate the total circuit resistance. Instead, the resistance of the capacitors and other circuit wiring (not necessarily at liquid hydrogen temperature) may dominate. Therefore, the resistance of 0.029 Ω may not be achievable in a practical sense.

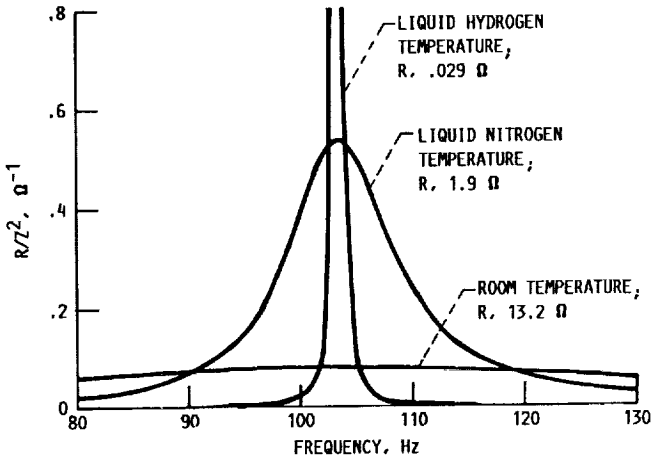

Figure 6.—Electrical circuit resistance divided by impedance squared as function of frequency for various temperatures. Inductance, 0.026 H; capacitance, 90 μF.

Tuning the Electromagnetic Damper Circuit

Tuning the electromagnetic damper circuit was complicated because the rotor had different but closely spaced critical speeds in the X and Y directions. Initially, the circuits were tuned such that the resonant frequencies of the X' and Y' circuits were equal to the frequencies of the critical speeds

for the X and Y directions, respectively. This, however, did not produce the lowest amplitude response. Therefore, to achieve the lowest amplitude response, the tuning of the electromagnetic damper circuit was determined by varying the capacitance to see which one produced the lowest amplitude response. The lowest amplitude response was achieved when the capacitance was approximately 90 μF on both the X' and Y' circuits.

In order to verify that the circuit was performing properly, a sinusoidal signal with amplitude of 1 V (peak to peak) was supplied to the circuit of figure 5 over a frequency range from 0 to 150 Hz, and the current flowing in the coils was measured as a function of frequency. The shaft and coils were constrained against lateral motion for this test. This was done for both the X' and Y' axes for capacitances of 90 and 100 μF. Figure 7 shows the results of this experiment for the 90 μF capacitance compared with the theoretical current ($I = E/Z$). The experimental curves show reasonably good agreement with the theoretical values and indicate satisfactory performance of the circuit and hardware. Note that the resonant frequency was 103.4 Hz for both the theoretical and experimental data. The current for capacitance values of 100 μF was similar to that for 90 μF. The resonant frequency was 98.2 Hz, as expected.

Undamped Unbalance Response (Baseline)

The experimental undamped response for the test rotor for the X and Y directions is shown in figure 8(a). These data were obtained with the damper turned off. The data are for an unbalance of 0.65 g-cm (0.09 oz-in.) applied at the rotor disk.

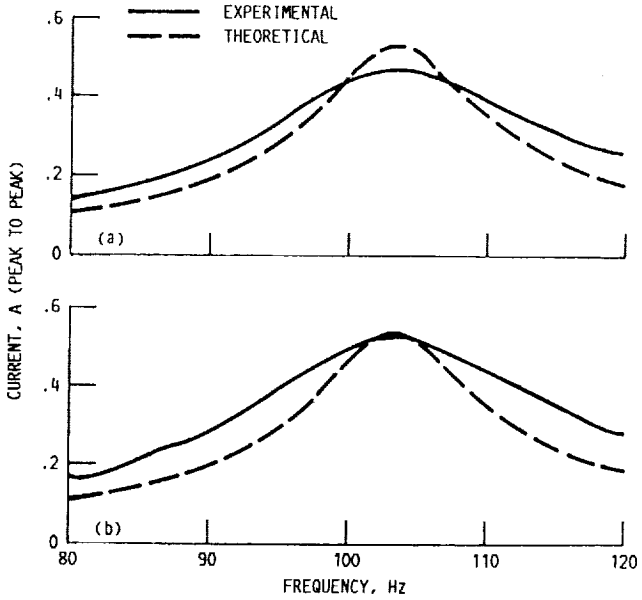

(a) X direction (current versus frequency).
(b) Y direction (current versus frequency).

Figure 7.—Comparison of actual current with theoretical current in tuned electromagnetic damper circuit. Liquid nitrogen temperature, −196 °C (−321 °F); capacitance, 90 μF; 1 V peak to peak impressed across circuit.

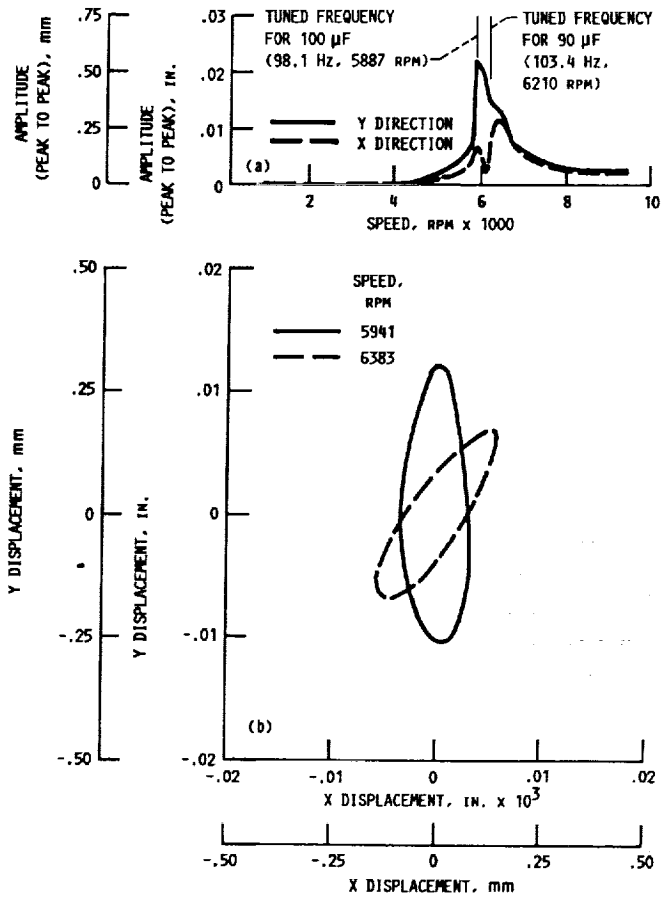

(a) Shaft amplitude as function of speed for X and Y directions.
(b) Undamped shaft orbits at critical speeds.

Figure 8.—Undamped rotor response (baseline).

This unbalance was used for all of the tests. The figure shows that the rotor has two closely spaced critical speeds. These were probably caused by nonuniform support stiffness and gyroscopic effects of the rotor. The closely spaced critical speeds (an unfortunate circumstance of the rig) complicated the evaluation of damper performance. The figure also indicates two critical speeds in the X direction at 5941 and 6383 rpm, with amplitudes of 0.15 and 0.28 mm (0.006 and 0.011 in.) peak to peak, respectively. One critical speed is indicated in the Y direction at 5941 rpm with an amplitude of 0.55 mm (0.022 in.) peak to peak. Figure 8(b) shows the undamped shaft orbits at the critical speeds. These data are the baseline against which the damper performance will be compared.

Damped Unbalance Response

Unbalance response tests were performed in which the electrical circuit for the damper was tuned to different frequencies using either 90 or 100 μF capacitors. The values of the tuned electrical circuit frequencies with respect to the undamped critical speeds are shown in figure 8(a). The 90 μF capacitors on both the X' and Y' axes tuned the system to the center of

the amplitude bandwidth (103.4 Hz, 6210 rpm) and the 100 μF capacitors on both the X' and Y' axes tuned the system to the peak amplitude frequency in the Y direction (98.1 Hz, 5887 rpm), as shown in the figure. Note that both the X' and Y' axes were tuned to the same frequency for each test.

Figure 9(a) shows the damped unbalance response with the electromagnetic damper turned on. The capacitance was 90 μF on both the X' and Y' axes, and the tuned frequency was 103.4 Hz (6210 rpm). The tuned frequency was approximately at the center of the amplitude bandwidth. This tuned frequency produced the most damping in both the X and Y directions. Figure 9(b) shows the damped shaft orbits at the critical speeds.

Figure 10(a) shows the damped unbalance response for 100 μF capacitors on both the X' and Y' axes, and the tuned frequency was 98.1 Hz (5887 rpm). Note that this frequency was close to the frequency of the maximum Y amplitude for the undamped case (fig. 8(a)). This tuned frequency did not produce as much overall damping as did the 103.1 Hz (90 μF) frequency. The damped shaft orbits at the critical speed for the 100 μF capacitance are shown in figure 10(b). Note that the damped critical speeds were approximately 175 to 300 rpm higher than for the undamped cases. This is because the amplitudes near the critical speed, where the damper was most effective, were reduced more than they were at the extremes of the amplitude bandwidth. The apparent upward shift in critical speed was therefore not due to any stiffening effect of the damper.

Figure 11(a) shows the undamped unbalance response compared with the electromagnetically damped response for the X direction. The figure indicates that the damper began to produce damping at approximately 5800 rpm (96.7 Hz) and

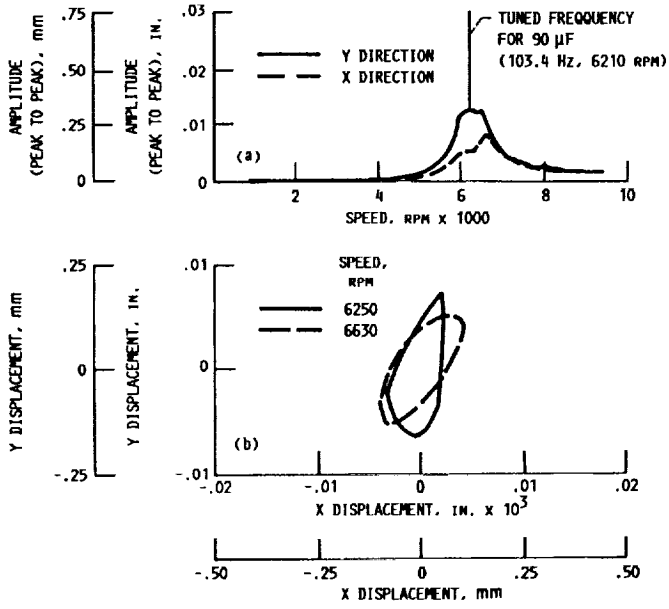

(a) Shaft amplitude as function of speed for X and Y directions.
(b) Damped shaft orbits at critical speeds.

Figure 9.—Damped unbalance response for 90 μF capacitors on X and Y axes.

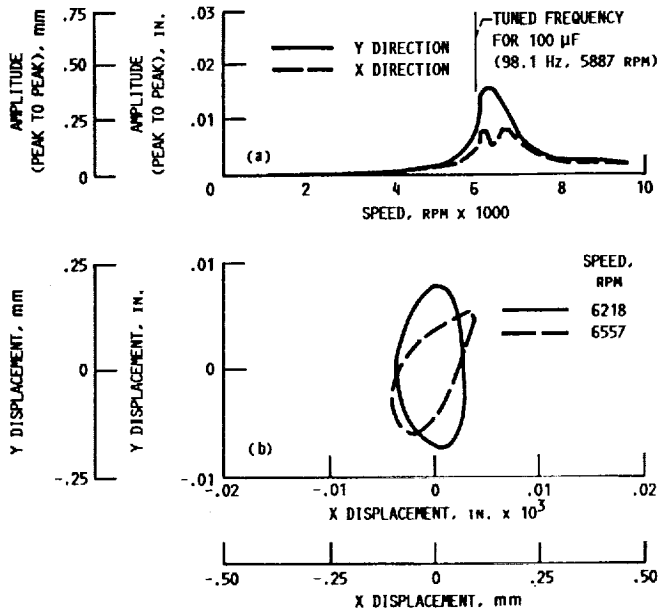

(a) Shaft amplitude as function of speed for X and Y directions.
(b) Damped shaft orbits at critical speeds.

Figure 10.—Damped unbalance response for 100 μF capacitors on X and Y axes.

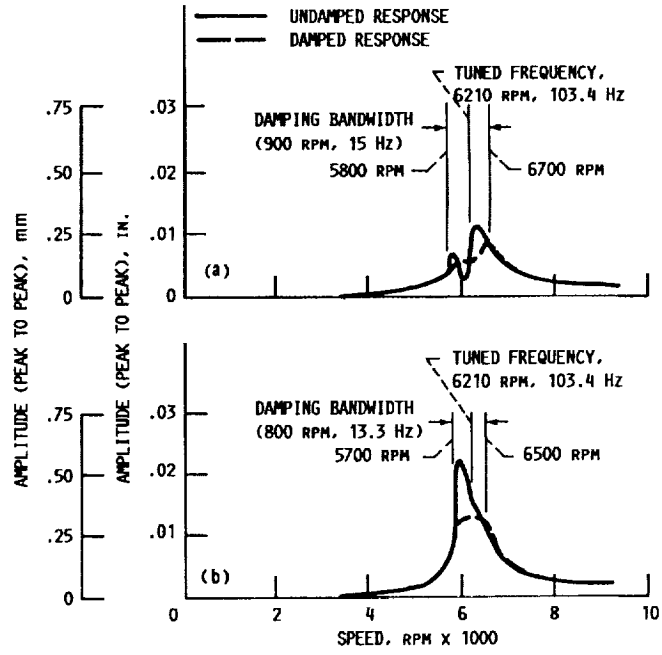

(a) X direction.
(b) Y direction.

Figure 11.—Comparison of undamped unbalance response with damped response for electromagnetic damper. Capacitance, 90 μF.

ceased to produce damping at approximately 6700 rpm (111.7 Hz). The difference between these two frequencies will be referred to as the damping bandwidth, as shown in the figure. This figure shows that the damping bandwidth was 900 rpm (15 Hz), and the center frequency for the damping bandwidth was 104.2 Hz. Note that the damper was tuned to 103.4 Hz, indicating that the damping bandwidth was nearly centered about the tuned frequency. The reduction of the maximum amplitude (X direction) between the undamped and damped response was 25 percent over the entire damping bandwidth but the reduction was 45 percent at the undamped critical speed (6383 rpm) (see fig. 11(a)). This suggests that the damper performance was greatly compromised for a broadband vibration or for closely spaced multimode vibrations, and was best suited for damping pure single-mode vibrations with narrow bandwidth.

Figure 11(b) shows the undamped unbalance response compared with the damped response for the Y direction. For this direction, the figure indicates that the damper produced damping between 5700 rpm (95 Hz) and 6500 rpm (108.3 Hz). The damping bandwidth for this direction was 800 rpm (13.3 Hz) and the center frequency for this bandwidth was 101.7 Hz (slightly less than the tuned frequency of 103.4 Hz). The reduction of the maximum amplitude (Y direction) was 40 percent over the entire damping bandwidth, and the reduction at the undamped critical speed (5941 rpm) was 47 percent (see fig. 11(b)). The damper performance was better in the Y direction than in the X direction. This was attributed to the fact that this mode did not have the double amplitude peaks as did the modes in the X direction. This again demonstrates that the damper performs better when damping pure single-mode vibrations.

Accurate comparisons between theoretical and experimental damping coefficients could not be made because the experimental data were complicated by the closely spaced modes of rotor vibration. Therefore, this report was limited to comparing the reduction of the peak amplitudes between undamped and damped conditions.

Figure 12(a) shows a comparison of the damped shaft orbit compared with the undamped orbit at the maximum X amplitude for the 90 μF case. Figure 12(b) shows the damped and undamped orbits at the maximum Y amplitude.

It should be noted that the electromagnetic damper used in these tests was not optimized. Damper performance can be improved by—

(1) Increasing the magnetic field strength through better arrangement of the magnets and by using more magnets;

(2) Packaging the coils more efficiently and seeking a better geometrical configuration for the coils; and

(3) Reducing the air gap between the coils and the magnets.

All three of these methods are dependent upon the shape and size of the available space envelope for any given application. This makes the damper configuration strongly dependent upon the application in which it is used.

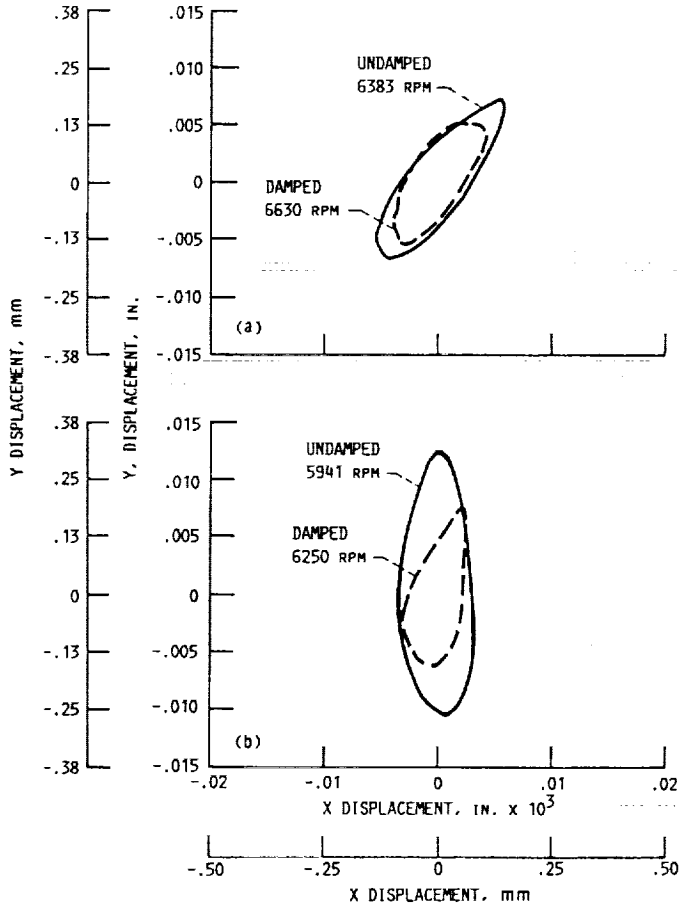

(a) Shaft orbits at maximum X amplitude.
(b) Shaft orbits at maximum Y amplitude.

Figure 12.—Comparison of undamped and damped shaft orbits for 90 μF capacitor.

Current Generated in Electromagnetic Damper Coils

The shaft amplitude and current generated in the electromagnetic damper coils for the X and Y directions for the 90 μF capacitors are shown in figure 13. These data were taken during the unbalance response tests. The curves show that the current flowing in the coils was a function of shaft amplitude because the shapes of the amplitude and current traces were similar. Note that the current has a sharp reduction at the high end of the damping bandwidth. Also, the current continued to increase for speeds above the tuned frequency because of the higher amplitudes at those speeds. The maximum current for the X direction was 1.22 A peak to peak at 6596 rpm (109.9 Hz). The shaft displacement and velocity at this speed were 0.20 mm (0.008 in.) peak to peak and 140 mm/sec (5.52 in./sec) peak to peak, respectively. The maximum current for the Y direction was 1.52 A peak to peak at 6210 rpm (103.4 Hz). The shaft displacement and velocity

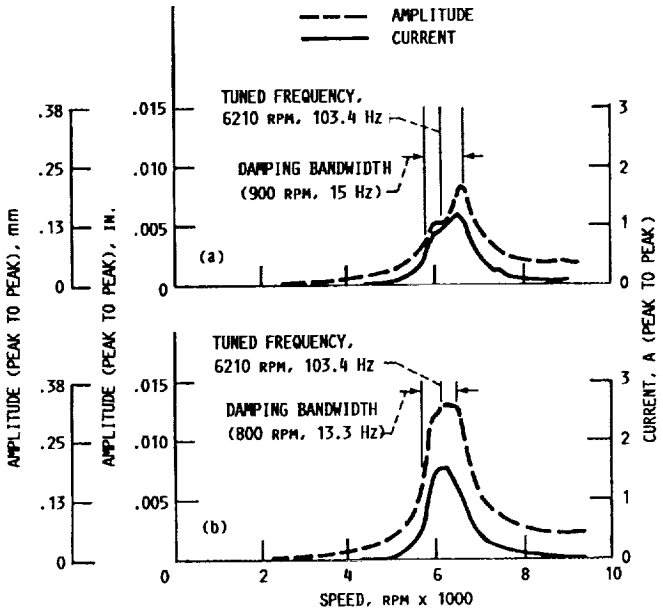

(a) *X* direction.
(b) *Y* direction.

Figure 13.—Shaft amplitude and current generated during unbalance response tests in electromagnetic damper. Capacitance, 90 μF.

at this speed were 0.33 mm (0.013 in.) peak to peak and 214 mm/sec (8.44 in./sec) peak to peak, respectively. Note that these velocities were calculated from the measured displacements.

The power dissipated in the damper coils can be calculated by using the current from figure 13(b). At 103.4 Hz (6210 rpm), where the maximum current of 1.52 A peak to peak (0.54 A rms) was generated in the coils, the power dissipated, (I^2R), was 0.55 W rms. The damping coefficient for this case as calculated from equation (6) was 96.7 N sec/m (0.55 lb sec/in.) at 6210 rpm (103.4 Hz).

In order to determine if the circuit was generating the correct voltage, a test was run in which the voltage was measured directly across the coils with the circuit open. Because the circuit was open, the damper did not produce damping during these tests. The theoretical voltage generated in the open circuit coils is given by equation (7). This equation gives the voltage across the coils and was used to calculate the theoretical open-circuit voltage in the coils. In this equation, the conductors are presumed to be straight. Because the conductors were actually in the form of a coil, they were curved rather than straight. This necessitated approximating an effective straight conductor length in the magnetic field. The effective conductor length in the magnetic field was approximately 20 mm (0.8 in.) and the effective number of conductors in the magnetic field was approximately 500. The magnetic field strength was 0.57 W/m^2 (5.7 kG). The values used for the velocities (v) in equation (7) were calculated from the experimental undamped amplitudes (*Y* direction). Figure 14 shows a comparison

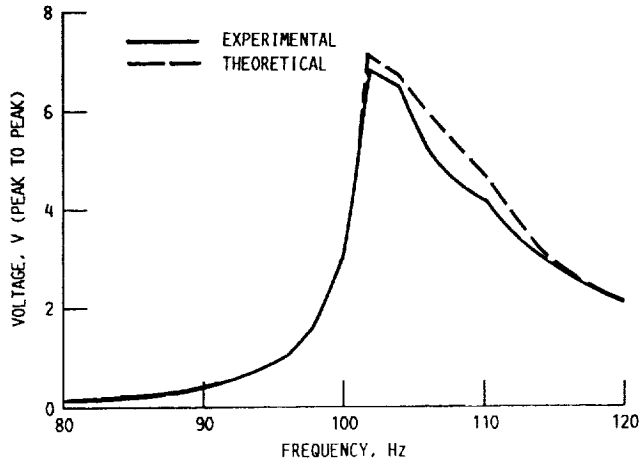

Figure 14.—Comparison of theoretical open-circuit voltage generated across damper coils to experimental voltage for undamped test (*Y* direction).

between the theoretical voltage (peak to peak) and the experimental (undamped) voltage generated across the damper coils for the open circuit. The figure shows good agreement between the theoretical and experimental undamped voltages, indicating that the damper was operating properly.

Summary of Results

Experiments were performed on a tuned electromagnetic vibration damper for damping rotor shaft vibrations in cryogenic turbomachinery. The tests consisted of operating an unbalanced rotor through its critical speed (5900 to 6400 rpm) and measuring the amplitude response for undamped and damped conditions at liquid nitrogen temperature (−196 °C, −321 °F).

The significant findings were as follows:

(1) The tuned electromagnetic damper provided a high degree of damping at the tuned frequency. However, the bandwidth over which the damping was effective was narrower than the amplitude response bandwidth for the rotor. Because of this, high amplitudes at the extremes of the amplitude response bandwidth remained undamped. This suggests that the tuned electromagnetic damper is well suited to damping single-mode vibrations of narrow bandwidth but is less effective in damping closely spaced multimode vibrations of broader bandwidth.

(2) For the *X* direction, the peak response over the entire damping bandwidth was reduced by approximately 25 percent, with the reduction at the undamped critical speed being 45 percent. For the *Y* direction, the peak response over the entire damping bandwidth was reduced by approximately 40 percent, with the reduction of peak amplitude at the undamped critical speed being 47 percent.

(3) The tuned electromagnetic damper requires cryogenic temperatures in order to be effective. The lower the

temperature the greater the damping produced at resonance. However, the bandwidth over which appreciable damping is obtained becomes narrower.

(4) The electromagnetic damper used in this research evolved from existing hardware. Therefore, the design of the damper and the general arrangement and configuration of the magnets and coils were not optimum. Damper performance can be improved by optimization of the coil and magnet geometry within the available space envelope.

(5) When the electromagnetic damper was used for damping rotating shaft vibrations, alternating current and voltage were generated in the damper coils. The phase relationship between alternating current and voltage significantly affects the performance of the damper. Therefore, this damper cannot be viewed as a simple linear device.

Lewis Research Center
National Aeronautics and Space Administration
Cleveland, Ohio, December 8, 1989

Appendix—Effect of Inductance, Resistance, and Capacitance on Current Flow in LRC Circuit

The effects of varying the inductance, resistance, capacitance, and frequency on the current generated in the circuit of figure 5 are shown in figure 15. Figure 15(a) shows that varying the capacitance while holding the resistance and inductance constant changes the resonant frequency of the circuit, but that the maximum current remains constant. Figure 15(b) shows that varying the inductance while holding the capacitance and resistance constant also changes the resonant frequency and again the maximum current remains constant. Figure 15(c) shows that changing the resistance while holding the capacitance and inductance constant changes the maximum current, but that the resonant frequency remains unchanged. Note that as the resistance decreases, the current increases sharply. The maximum current at the circuit's resonant frequency is inversely proportional to the circuit's resistance. This is because at resonance the inductive effects are cancelled by the capacitive effects and the circuit becomes purely resistive. Reference 7 gives a detailed discussion of this phenomenon.

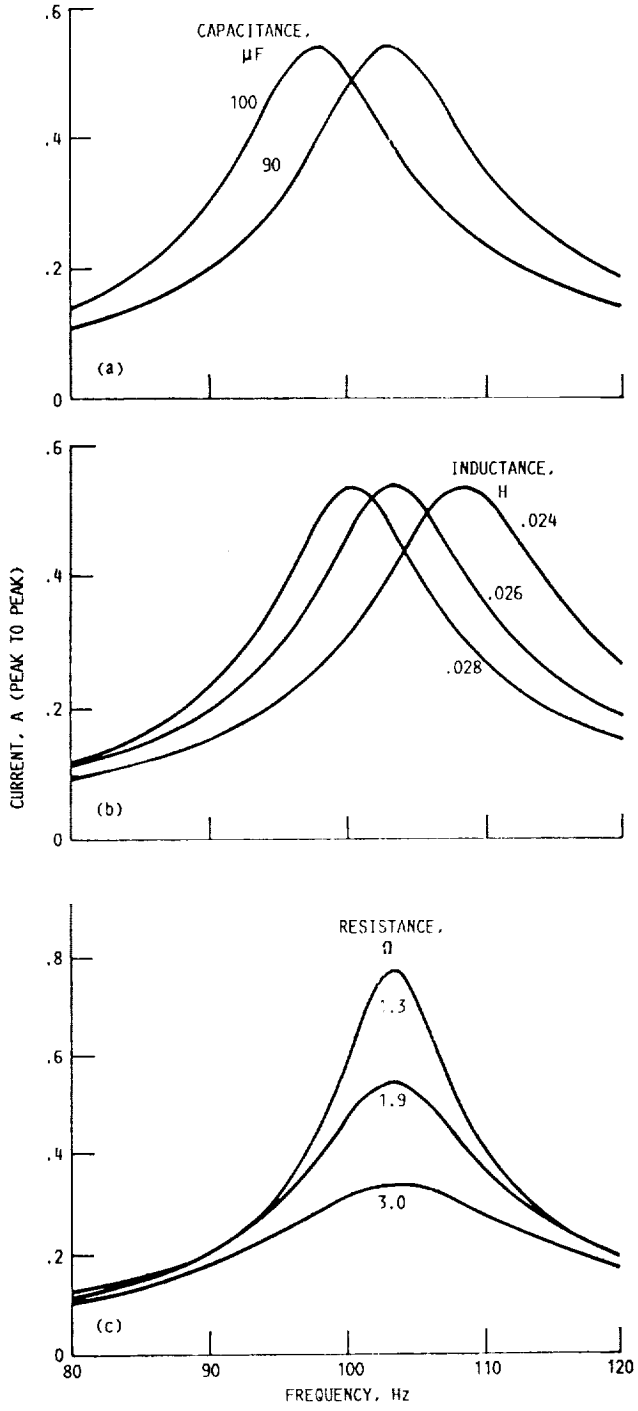

(a) Current versus frequency for various capacitances. Resistance, 1.9 Ω; inductance, 0.026 H.

(b) Current versus frequency for various inductances. Resistance, 1.9 Ω; capacitance, 90 μF.

(c) Current versus frequency for various resistances. Inductance, 0.026 H; capacitance, 90 μF.

Figure 15.—Effect of capacitance, inductance, and resistance on current in tuned electromagnetic damper circuit. Data are for 1 V peak to peak impressed across circuit.

References

1. Ek, M.C.: Solution of the Subsynchronous Whirl Problem in the High Pressure Hydrogen Turbomachinery of the Space Shuttle Main Engine. AIAA Paper 78-1002, July 1978.
2. Gunter, E.J.; Humphris, R.R.; and Severson, S.J.: Design Study of Magnetic Eddy-Current Vibration Suppression Dampers For Application To Cryogenic Turbomachinery. (UVA/528210/MAE 84/101, Rotor Dynamics Lab, University of Virginia, Charlottesville; NASA Grant NAG3-263) NASA CR-173273, 1983, pp. 6-1 to 6-3.
3. Harris, C.M.; and Crede, C.E., eds.: Shock and Vibration Handbook, Second ed. McGraw Hill, 1976, pp. 32-33.
4. Shortley, G.; and Williams, D.: Elements of Physics, Second ed. Prentice-Hall, Inc., 1955, p. 765.
5. Shortley, G.; and Williams, D.: op. cit., p. 764.
6. Shortley, G.; and Williams, D.: op. cit., p. 728.
7. Shortley, G.; and Williams, D.: op. cit., pp. 763-767.

NASA
National Aeronautics and Space Administration

Report Documentation Page

1. Report No.	2. Government Accession No.	3. Recipient's Catalog No.
NASA TP-3005		

4. Title and Subtitle	5. Report Date
Experimental Evaluation of a Tuned Electromagnetic Damper for Vibration Control of Cryogenic Turbopump Rotors	June 1990
	6. Performing Organization Code

7. Author(s)	8. Performing Organization Report No.
Eliseo DiRusso and Gerald V. Brown	E-5012
	10. Work Unit No. 582-01-31

9. Performing Organization Name and Address	11. Contract or Grant No.
National Aeronautics and Space Administration Lewis Research Center Cleveland, Ohio 44135-3191	
	13. Type of Report and Period Covered: Technical Paper

12. Sponsoring Agency Name and Address	14. Sponsoring Agency Code
National Aeronautics and Space Administration Washington, D.C. 20546-0001	

15. Supplementary Notes

16. Abstract

Experiments were performed on a passive tuned electromagnetic damper that could be used for damping rotor vibrations in cryogenic turbopumps for rocket engines. The tests were performed in a rig that used liquid nitrogen to produce cryogenic turbopump temperatures. This damper is most effective at cryogenic temperatures and is not a viable damper at room temperature. The unbalanced amplitude response of the rotor shaft was measured for undamped (baseline) and damped conditions at the critical speeds of the rotor (approximately 5900 to 6400 rpm) and the data were compared. The tests were performed for a speed range between 900 and 10 000 rpm. The tests revealed that the damper is very effective for damping single-mode narrow bandwidth amplitude response but is less effective in damping broadband response or multimode amplitude response.

17. Key Words (Suggested by Author(s))	18. Distribution Statement
Vibration control; Damping; Rotor dynamics; Magnetic bearings; Active control	Unclassified – Unlimited Subject Category 07

19. Security Classif. (of this report)	20. Security Classif. (of this page)	21. No. of pages	22. Price*
Unclassified	Unclassified	17	A03

*For sale by the National Technical Information Service, Springfield, Virginia 22161